Letter Vol. 43, No. 19 / 1 October 2018 / Optics Letters 4607

Optics Letters

Measuring the orbital angular momentum spectrum with a single point detector

SHIKANG LI, PENG ZHAO, XUE FENG,* KAIYU CUI, FANG LIU, WEI ZHANG, AND YIDONG HUANG

Department of Electronic Engineering, Tsinghua University, Beijing 100084, China
**Corresponding author: x-feng@tsinghua.edu.cn*

Received 29 May 2018; revised 18 August 2018; accepted 18 August 2018; posted 22 August 2018 (Doc. ID 332544); published 19 September 2018

It is tough work to measure the orbital angular momentum (OAM) spectrum due to the requirement of a reference light or photodetector arrays, while measuring the spin angular momentum (SAM) is readily convenient and matured. In this work, the so-called OAM–SAM nonseparable states are employed, and the OAM spectrum can be obtained only by measuring the Stokes parameters of an arbitrary light beam with low loss noncascading structure and a single point detector. According to the experimental results, the fidelity of the measured OAM spectrum can be as high as 95.2% and 94.3% for OAM eigenstates and superposed states, respectively.

OCIS codes: (050.4865) Optical vortices; (260.5430) Polarization; (260.6042) Singular optics.

https://doi.org/10.1364/OL.43.004607

Verified by Allen *et al.* in 1992, the orbital angular momentum (OAM) can be well defined by a Laguerre–Gaussian light beam with azimuthal phase term of $\exp(il\phi)$ [1], which can also be treated as the lth eigenstate of an infinite Hilbert space. One of the unique characteristics of OAM beams is their high dimensional nature, which has attracted research interest for various applications of free space [2] and on-chip [3] optical communications, optical imaging [4], and quantum information [5], including high performance quantum metrology [6], new quantum communication protocols [7], quantum dense coding [8], quantum simulation [9], and quantum cryptography [10]. For these applications, identifying the OAM states carried by an arbitrary light beam is an essential and significant problem. In some earlier works, the OAM topological charge is extracted by analyzing intensity distributions after passing some optical elements, such as double slits [11], triangular apertures [12], single slits [13], wedged flat [14], and annular gratings [15]. For these methods, it is hard to measure the whole OAM spectrum since the detected charge range is limited by a certain optical element. Recently, several improved approaches for measuring the OAM spectrum emerged; the operation principles include the rotational Doppler effect [16] and interference pattern analysis [17,18]. However, since a reference light beam is required, these methods cannot be applied to single photon measurement. Another approach toward the OAM spectrum is an OAM sorter, which is available for single photons with high performance and low insertion loss. Representative methods are based on cascaded OAM beamsplitters [19,20] and optical field transformation [21], which is further developed to reduce the overlap between adjacent eigenstates of OAM [22] and minimize the device footprint [23]. Most recently, the complete OAM density matrix of a single photon can be characterized [24]. Furthermore, with the help of an interferometer, the OAM spectrum of parametric downconverted photons with high Schmidt number has been successfully extracted [25]. However, either a charge coupled device (CCD) or photodetector array is still required, which is obviously not cost effective. As mentioned above, how to identify the OAM spectrum with a single point detector and without a reference light beam is still an open question.

In this work, an approach with a single point detector is demonstrated to measure the OAM spectrum. We further offer a method to determine the mean OAM value under the same experimental setup. In our approach, the OAM state under test is first converted to the OAM–spin angular momentum (OAM–SAM) nonseparable state [26] and consequently the OAM spectrum is extracted by measuring the spin angular momentum (SAM). The OAM–SAM nonseparable state describes a vectorial vortex beam whose state vector cannot be represented by the direct product of OAM and SAM components. Though exhibiting no violation of classical behaviors, the OAM–SAM nonseparable state provides an additional approach in quantum metrology [27]. A typical OAM–SAM nonseparable state can be prepared by passing a linear polarized light beam through a q-plate [28], where two OAM eigenstates are interacted with the SAM. In our proposal, a modified Mach–Zehnder (M-Z) interferometer is adopted to prepare the required OAM–SAM nonseparable state. The SAM of a light beam can be identified with the standard Stokes parameter measurement method. Thus, with OAM–SAM nonseparable state, the OAM spectrum can be determined without CCD camera and reference light. According to the experimental results, the fidelity of the measured OAM spectrum can be 85.3–95.2% and 84.3–94.3% for eigenstates and superposed states, respectively.

The schematic experimental setup is shown in Fig. 1. The fundamental Gaussian mode at 1550 nm output from the laser (RIO Orion) is injected into the system through a collimator. A polarizer (P1) is adopted to ensure the desired linear polarization state. With a spatial light modulator (SLM, Holoeye Pluto) and a beamsplitter, the fundamental Gaussian mode is converted to the initial OAM state $|L\rangle = \sum m_l |l\rangle, \sum |m_l|^2 = 1$ with a checkerboard method. After that, the OAM–SAM nonseparable state is prepared through a M-Z interferometer, which consists of two polarization beamsplitters (PBSs) as well as one dove prism (DP1 and DP2) in each arm.

A half wave plate (HWP) is utilized to rotate the polarization with the angle of 45° according to the polarization axis of PBS1; thus the modified OAM–SAM state $|\psi\rangle = |L\rangle \otimes |S\rangle$ (with $|S\rangle = (|H\rangle + |V\rangle)/\sqrt{2}$) is prepared. Then, state $|\psi\rangle$ is injected into the M-Z interferometer. DP1 is fixed while the rotation angle α of DP2 can be varied by a stepper motor rotation mount (Thorlabs) with accuracy of $\pm 0.14°$. The state evolution through the M-Z interferometer can be described as a unitary operator of $\hat{U}(\alpha)$ with $\hat{U}(\alpha)|l\rangle \otimes |S\rangle = |l\rangle \otimes (|H\rangle + \exp(-2i\alpha l)|V\rangle)/\sqrt{2}$. Thus, the SAM state and OAM state would be classically nonseparable by $\hat{U}(\alpha)$ and the density matrix of the state after the M-Z interferometer is

$$\begin{aligned}\hat{\rho}_{ns} &= \hat{U}(\alpha)\hat{\rho}_0 \hat{U}^\dagger(\alpha) \\ &= \frac{1}{2}\sum |m_l|^2 |l\rangle\langle l| \otimes (|H\rangle\langle H| + |V\rangle\langle V| \\ &\quad + \exp(-2i\alpha l)|V\rangle\langle H| + \exp(2i\alpha l)|H\rangle\langle V|), \end{aligned} \quad \textbf{(1)}$$

where $\hat{\rho}_0 = |\psi\rangle\langle\psi|$ is the density matrix of the OAM–SAM state before the M-Z interferometer. The required information on SAM can be obtained by measuring the second and third Stokes parameters, which can be expressed by traces of the first and second Pauli matrices acting on the final SAM unconditional density matrix:

$$\langle\hat{\sigma}_x\rangle = Tr(\hat{\rho}_{ns}\hat{\sigma}_x) = \sum |m_l|^2 \cos 2\alpha l, \quad \textbf{(2)}$$

$$\langle\hat{\sigma}_y\rangle = Tr(\hat{\rho}_{ns}\hat{\sigma}_y) = -\sum |m_l|^2 \sin 2\alpha l, \quad \textbf{(3)}$$

where $\hat{\sigma}_x = |H\rangle\langle V| + |V\rangle\langle H|$ and $\hat{\sigma}_y = -i|H\rangle\langle V| + i|V\rangle\langle H|$ are the second and third Stokes parameters in polarization degrees of freedom, respectively. Here, Pauli matrices are realized by a tunable liquid crystal delay line (DL, LCC-1223C, Thorlabs) and a polarizer (P2) after it. The DL serves as a tunable wave plate since it can introduce arbitrary phase delay with value from 0 to 2π only for the polarization component parallel to the slow axis. In practice, the phase delay of the DL is set to be 0 or $\pi/2$ to detect linear diagonal or right circular polarization states, respectively, which correspond to the second or third Stokes parameter. The polarization orientation of P2 is fixed at 45° according to the polarization axis of PBS2. Additionally, the tunable DL also serves to compensate the optical path difference between the two arms of the interferometer. From Eqs. (2) and (3), the relation of $f(\alpha) = \langle\hat{\sigma}_x\rangle - i\langle\hat{\sigma}_y\rangle = \sum |m_l|^2 \exp(i2\alpha l)$ can be readily found. Thus, the OAM spectrum coefficients $\{|m_l|^2\}$ can be calculated by a discrete Fourier transformation (DFT) algorithm after measuring a series of Stokes parameters with varied α from 0 to π. In detail, it is $|m_l|^2 = \sum f(\alpha)\exp(-i2\alpha l)$.

Several experiments have been carried out to verify our proposed approach. First, the input OAM states under test are eigenstates with l ranges from −5 to 4. The measured spectra of these states are shown in Fig. 2(a). To evaluate the accuracy, a parameter of fidelity $\mathcal{F}$ is adopted, and the definition is

$$\mathcal{F} = \frac{Tr(M'P)}{\sqrt{Tr(M'M)Tr(P'P)}}, \quad \textbf{(4)}$$

where M and P denote the measured and preset OAM amplitude spectra, respectively. The energy normalization is also done in Eq. (4). For the results shown in Fig. 2(a), the corresponding fidelity is 85.3% ($l = 1$) to 95.2% ($l = -3$). Figure 2(b) shows measured spectrum for eigenstate $l = -4$ with fidelity of 92.1%.

Next, the input states under test are prepared as the OAM superposed states of $l = -6, 3, 6$ with energy ratio of 1:1:1, and $l = -4, 4, 6$ with energy ratio of 2:1:2, respectively. The measured intensity patterns are shown in Figs. 3(a) and 3(c). The intensity patterns are measured by a CCD camera. Figures 3(b) and 3(d) show the measured OAM spectra corresponding to Figs. 3(a) and 3(c) with fidelity of 87.0% and 85.5%, respectively. The gray bars and black bars denote the preset and measured OAM spectra, respectively.

Moreover, much wider OAM spectra have been prepared and measured. The superposed OAM state is prepared by setting the phase pattern on the SLM as in Fig. 4(a). Red and blue colors denote 0 and π phase delay, respectively. The brightness indicates energy intensity, which is exactly a Gaussian envelope. The intensity modulation is achieved by the checkerboard method. Due to the segment azimuthal phase distribution, the preset OAM state can be represented as follows:

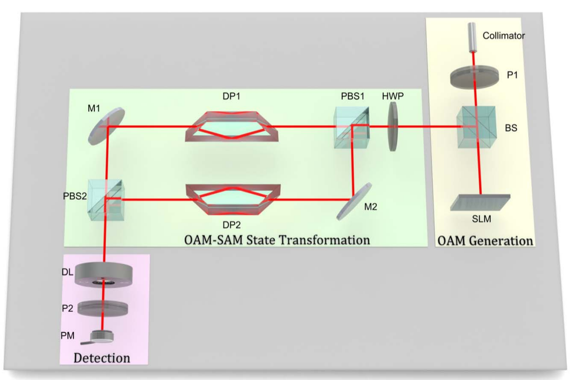

Fig. 1. Scheme of experimental setup. P, polarizer; BS, beamsplitter; SLM, spatial light modulator; HWP, half wave plate; M, mirror; DP, dove prism; DL, delay line; PM, power meter.

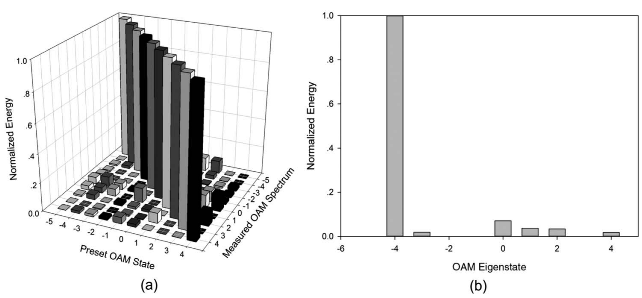

Fig. 2. (a) Measured OAM spectrum of eigenstates with l ranges from −5 to 4. The fidelity of these results is 85.3–95.2%. (b) Typical measured spectrum of OAM eigenstate with $l = -4$.

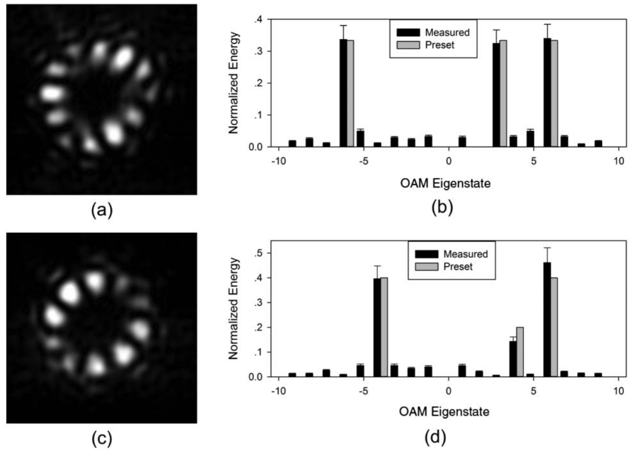

Fig. 3. Intensity patterns of OAM superposed states and measured OAM spectrum. (a) Intensity pattern of superposed state of $l = -6$, $l = 3$, and $l = 6$ with energy ratio of 1:1:1. (c) Intensity pattern of superposed state of $l = -4$, $l = 4$, and $l = 6$ with energy ratio of 2:1:2. (b) and (d) Preset (gray) and measured (black) OAM spectra corresponding to OAM states in (a) and (c), with fidelity of 87.0% and 85.5%, respectively.

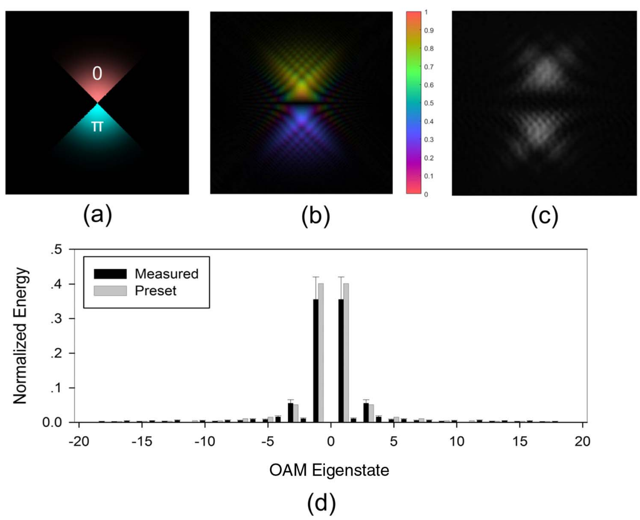

Fig. 4. (a) Phase pattern on SLM to generate wide OAM spectrum. Red and blue colors denote 0 and π phase delay, respectively. (b) Field simulated through Huygens–Fresnel theory. (c) Intensity pattern measured by CCD camera. (d) Measured OAM spectrum while the gray bars and black bars are the preset and measured OAM spectra. The corresponding spectrum fidelity is 94.3%.

$$|L\rangle = \frac{2}{\pi}\sum_{n=1}^{\infty}\frac{1}{2n-1}(|2n-1\rangle - |-2n+1\rangle).$$

Figure 4(b) is the intensity pattern simulated by MATLAB through Huygens–Fresnel theory while Fig. 4(c) is the intensity pattern measured by the CCD camera. In Fig. 4(b), brightness indicates light intensity and the color bar represents phase in units of 2π. When the preset OAM spectrum is symmetric, only $\langle\hat{\sigma}_x\rangle$ values are required. Figure 4(d) shows the measured OAM spectrum, where the gray bars and black bars are the preset and measured OAM spectra, which is exactly the Fourier transformation of the series of measured $\langle\hat{\sigma}_x\rangle$ values. The corresponding fidelity is 94.3%.

The experimental errors are mainly attributed to the polarization effect of the dove prism and beam misalignment. The polarization state of the incident light beam is slightly modulated by the dove prism (Thorlabs PS992M). The worst situation occurs when α equals 45° [29] where ~10% of the polarization state is changed. However, this influence can be eliminated by using dove prisms with larger base angle instead. The beam misalignment would cause mode cross talk [30] especially for superposed OAM states. With the checkerboard method for SLM coding, the mode purity of OAM states can be as high as 97% according to previous work [31]. Thus, the error of OAM state generation can be ignored.

Finally, it should be noticed that Eqs. (2) and (3) are even and odd functions of α, respectively. In practice, $2N$ SAM measurements are required to reconstruct $2N$ OAM spectrum coefficients $\{|m_l|^2\}$ from $l = -N$ to $l = N-1$. Though same number of measurements are required compared with earlier approaches adopting $2N$ specially designed holograms [5], only one dove prism is needed in our proposal. Since copies of the photon under test are required for intensity accumulation on an electron-multiplying CCD in previous works [24,25], we suggest that our low loss approach could be extended to single photon OAM spectrum analysis also with a proper amount of photon copies. As proposed in earlier work [27], if only the OAM mean value $\langle\hat{L}_z\rangle$ (with $\hat{L}_z|l\rangle = l|l\rangle$) of the initial OAM state is concerned, the measurement can be simplified. Here, we offer an approach to determine the mean OAM value under the same experimental setup. When the rotation angle α of the dove prism shown in Fig. 1 is sufficiently small and fixed, Eqs. (2) and (3) can be extended in polynomial function form:

$$\langle\hat{\sigma}_x\rangle = 1 - 2\alpha^2\langle L_z^2\rangle + O(\alpha^4)$$
$$\langle\hat{\sigma}_y\rangle = -2\alpha\langle L_z\rangle + \frac{4}{3}\alpha^3\langle L_z^3\rangle + O(\alpha^5). \quad \textbf{(5)}$$

With simple calculation, we can obtain

$$\arctan\left(\frac{-\langle\hat{\sigma}_y\rangle}{\langle\hat{\sigma}_x\rangle}\right)$$
$$= 2\alpha\langle\hat{L}_z\rangle - 8\alpha^3\left(\frac{1}{6}\langle\hat{L}_z^3\rangle + \frac{1}{3}\langle\hat{L}_z\rangle^3 - \frac{1}{2}\langle\hat{L}_z\rangle\langle\hat{L}_z^2\rangle\right) + O(\alpha^5). \quad \textbf{(6)}$$

Equation (6) shows that the OAM mean value of $\langle\hat{L}_z\rangle$ could be obtained with two measured Stokes parameters, and the accuracy is $O(\alpha^3)$ at least. Actually, the term of $\frac{1}{6}\langle\hat{L}_z^3\rangle + \frac{1}{3}\langle\hat{L}_z\rangle^3 - \frac{1}{2}\langle\hat{L}_z\rangle\langle\hat{L}_z^2\rangle$ is quite small except for some extreme situations so that the accuracy is about $O(\alpha^5)$ for most cases. Figure 5 shows experimental results on OAM mean value measurements with our approach. Both eigenstates and superposed states are employed to obtain various OAM mean values ranging from −5 to 6. The superposed states are combinations of two OAM eigenstates. The black dashed line with a slope of 1 denotes the ideal result corresponding to preset states. The red markers and dotted line denote experimental results on eigenstates while the blue markers and solid line represent experimental results on superposed states. The zero mean value point is only used for

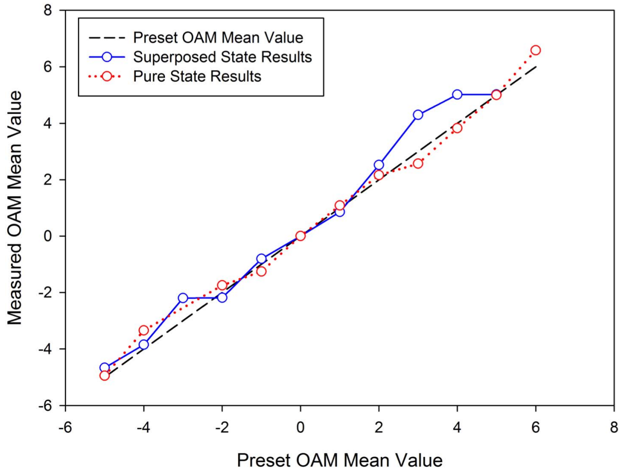

Fig. 5. Measured OAM mean value. The black dashed line with a slope of 1 denotes the ideal result corresponding to preset states. The red markers and dotted line denote experimental results on eigenstates while the blue markers and solid line represent experimental results on superposed states. The average relative errors for eigenstates and superposed states are 9.2% and 15.9%.

calibration. The average relative errors of measured OAM mean value are 9.2% and 15.9% for eigenstates and superposed states, respectively.

In this work, an approach with a single point detector is demonstrated to measure the OAM spectrum carried by paraxial light beams. Since the OAM–SAM nonseparable states are employed, there is no requirement on reference light and photodetector arrays. The fidelity values of measured OAM spectra are 95.2% and 94.3% for OAM eigenstates and superposed states, respectively. Furthermore, the OAM mean value can also be obtained with the same setup.

The achieved measurement accuracy in this work suffers from the angle accuracy of the dove prism. One possible improvement is employing a more stable Sagnac structure [32]. After improving the reliability of Dove prisms [33], our approach is potential for a cost-effective and compact OAM spectrum analyzer. The required SAM measurements can be further reduced with a compressed sensing method [34]. Finally, we believe that this work is a good effort to fully identify the information encoded on high-dimensional degrees of freedom (OAM) by measuring the low-dimensional observable (SAM), which would be interesting for nondestructive measurements.

Funding. National Natural Science Foundation of China (NSFC) (61675112, 61621064); National Basic Research Program of China (2013CBA01704, 2013CB328704).

REFERENCES

1. L. Allen, M. W. Beijersbergen, R. J. C. Spreeuw, and J. P. Woerdman, Phys. Rev. A **45**, 8185 (1992).
2. J. Wang, J.-Y. Yang, I. M. Fazal, N. Ahmed, Y. Yan, H. Huang, Y. Ren, Y. Yue, S. Dolinar, M. Tur, and A. E. Willner, Nat. Photonics **6**, 488 (2012).
3. D. Zhang, X. Feng, and Y. Huang, Opt. Express **20**, 26986 (2012).
4. N. Uribe-Patarroyo, A. Fraine, D. S. Simon, O. Minaeva, and A. V. Sergienko, Phys. Rev. Lett. **110**, 043601 (2013).
5. A. Mair, A. Vaziri, G. Weihs, and A. Zeilinger, Nature **412**, 313 (2001).
6. R. Fickler, R. Lapkiewicz, W. N. Plick, M. Krenn, C. Schaeff, S. Ramelow, and A. Zeilinger, Science **338**, 640 (2012).
7. M. Malik, M. Erhard, M. Huber, M. Krenn, R. Fickler, and A. Zeilinger, Nat. Photonics **10**, 248 (2016).
8. F. Wang, M. Erhard, A. Babazadeh, M. Malik, M. Krenn, and A. Zeilinger, Optica **4**, 1462 (2017).
9. X.-W. Luo, X. Zhou, C.-F. Li, J.-S. Xu, G.-C. Guo, and Z.-W. Zhou, Nat. Commun. **6**, 7704 (2015).
10. A. Sit, F. Bouchard, R. Fickler, J. Gagnon-Bischoff, H. Larocque, K. Heshami, D. Elser, C. Peuntinger, K. Günthner, B. Heim, C. Marquardt, G. Leuchs, R. W. Boyd, and E. Karimi, Optica **4**, 1006 (2017).
11. H. I. Sztul and R. R. Alfano, Opt. Lett. **31**, 999 (2006).
12. J. M. Hickmann, E. J. S. Fonseca, W. C. Soares, and S. Chávez-Cerda, Phys. Rev. Lett. **105**, 053904 (2010).
13. D. P. Ghai, P. Senthilkumaran, and R. S. Sirohi, Opt. Lasers Eng. **47**, 123 (2009).
14. B. Khajavi and E. J. Galvez, Opt. Lett. **42**, 1516 (2017).
15. S. Zheng and J. Wang, Sci. Rep. **7**, 40781 (2017).
16. H.-L. Zhou, D.-Z. Fu, J.-J. Dong, P. Zhang, D.-X. Chen, X.-L. Cai, F.-L. Li, and X.-L. Zhang, Light Sci. Appl. **6**, e16251 (2017).
17. A. D'Errico, R. D'Amelio, B. Piccirillo, F. Cardano, and L. Marrucci, Optica **4**, 1350 (2017).
18. P. Zhao, S. Li, X. Feng, K. Cui, F. Liu, W. Zhang, and Y. Huang, Opt. Lett. **42**, 1080 (2017).
19. J. Leach, M. J. Padgett, S. M. Barnett, S. Franke-Arnold, and J. Courtial, Phys. Rev. Lett. **88**, 257901 (2002).
20. S. Wei, S. K. Earl, X.-C. Yuan, S. S. Kou, and J. Lin, "Active sorting of orbital angular momentum states of light with cascaded tunable resonators," arXiv: 1704.01703 [physics] (2017).
21. G. C. G. Berkhout, M. P. J. Lavery, J. Courtial, M. W. Beijersbergen, and M. J. Padgett, Phys. Rev. Lett. **105**, 153601 (2010).
22. M. Mirhosseini, M. Malik, Z. Shi, and R. W. Boyd, Nat. Commun. **4**, 2781 (2013).
23. S. Lightman, G. Hurvitz, R. Gvishi, and A. Arie, Optica **4**, 605 (2017).
24. M. Mirhosseini, O. S. Magaña-Loaiza, C. Chen, S. M. Hashemi Rafsanjani, and R. W. Boyd, Phys. Rev. Lett. **116**, 130402 (2016).
25. G. Kulkarni, R. Sahu, O. S. Magaña-Loaiza, R. W. Boyd, and A. K. Jha, Nat. Commun. **8**, 1054 (2017).
26. E. Karimi and R. W. Boyd, Science **350**, 1172 (2015).
27. B. Piccirillo, S. Slussarenko, L. Marrucci, and E. Santamato, Nat. Commun. **6**, 8606 (2015).
28. L. Marrucci, C. Manzo, and D. Paparo, Phys. Rev. Lett. **96**, 163905 (2006).
29. M. J. Padgett and J. P. Lesso, J. Mod. Opt. **46**, 175 (1999).
30. M. V. Vasnetsov, V. A. Pas'ko, and M. S. Soskin, New J. Phys. **7**, 46 (2005).
31. A. Forbes, A. Dudley, and M. McLaren, Adv. Opt. Photon. **8**, 200 (2016).
32. F.-X. Wang, W. Chen, Y.-P. Li, G.-W. Zhang, Z.-Q. Yin, S. Wang, G.-C. Guo, and Z.-F. Han, Opt. Express **25**, 24946 (2017).
33. M. P. J. Lavery, A. Dudley, A. Forbes, J. Courtial, and M. J. Padgett, New J. Phys. **13**, 093014 (2011).
34. D. L. Donoho, IEEE Trans. Inf. Theory **52**, 1289 (2006).